ORIGINAL ARTICLE

Projected Changes in Climate Extremes Using CMIP6 Simulations Over SREX Regions

Mansour Almazroui[1,2] · Fahad Saeed[3] · Sajjad Saeed[4,5] · Muhammad Ismail[1] · Muhammad Azhar Ehsan[6] · M. Nazrul Islam[1] · Muhammad Adnan Abid[4] · Enda O'Brien[7] · Shahzad Kamil[8] · Irfan Ur Rashid[8] · Imran Nadeem[9]

Abstract

This paper presents projected changes in extreme temperature and precipitation events by using Coupled Model Intercomparison Project phase 6 (CMIP6) data for mid-century (2036–2065) and end-century (2070–2099) periods with respect to the reference period (1985–2014). Four indices namely, Annual maximum of maximum temperature (TXx), Extreme heat wave days frequency (HWFI), Annual maximum consecutive 5-day precipitation (RX5day), and Consecutive Dry Days (CDD) were investigated under four socioeconomic scenarios (SSP1-2.6; SSP2-4.5; SSP3-7.0; SSP5-8.5) over the entire globe and its 26 Special Report on Managing the Risks of Extreme Events and Disasters to Advance Climate ChangeAdaptation (SREX) regions. The projections show an increase in intensity and frequency of hot temperature and precipitation extremes over land. The intensity of the hottest days (as measured by TXx) is projected to increase more in extratropical regions than in the tropics, while the frequency of extremely hot days (as measured by HWFI) is projected to increase more in the tropics. Drought frequency (as measured by CDD) is projected to increase more over Brazil, the Mediterranean, South Africa, and Australia. Meanwhile, the Asian monsoon regions (i.e., South Asia, East Asia, and Southeast Asia) become more prone to extreme flash flooding events later in the twenty-first century as shown by the higher RX5day index projections. The projected changes in extremes reveal large spatial variability within each SREX region. The spatial variability of the studied extreme events increases with increasing greenhouse gas concentration (GHG) and is higher at the end of the twenty-first century. The projected change in the extremes and the pattern of their spatial variability is minimum under the low-emission scenario SSP1-2.6. Our results indicate that an increased concentration of GHG leads to substantial increases in the extremes and their intensities. Hence, limiting CO_2 emissions could substantially limit the risks associated with increases in extreme events in the twenty-first century.

Keywords CMIP6 models · Climate change · Climate extremes · Floods · Droughts · Heat waves

✉ Mansour Almazroui
mansour@kau.edu.sa

[1] Centre of Excellence for Climate Change Research/ Department of Meteorology, King Abdulaziz University, Jeddah 21589, Saudi Arabia

[2] Climatic Research Unit, School of Environmental Sciences, University of East Anglia, Norwich, UK

[3] Climate Analytics, Berlin, Germany

[4] Earth System Physics Section, The Abdus Salam International Centre for Theoretical Physics (ICTP), Trieste, Italy

[5] Department of Earth and Environmental Sciences, University of Leuven (KU Leuven), Leuven, Belgium

[6] International Research Institute for Climate and Society (IRI), The Earth Institute, Columbia University, Palisades, NY, USA

[7] Irish Centre for High-End Computing, Galway, Ireland

[8] Pakistan Meteorological Department, Climate Change Impact and Integration Cell (CIIC), Islamabad, Pakistan

[9] Institute of Meteorology and Climatology, University of Natural Resources and Life Sciences, Vienna, Austria

1 Introduction

Over the last 50 years (1970–2019), precipitation related extremes have resulted in many casualties, and caused enormous socioeconomic damage. The death toll from storms was over 577,000; with a further 58,700 from floods; 650,000 from droughts, and 55,700 from extreme temperatures (WMO 2021). Moreover, the last-two decades were the warmest in the entire 140-year long National Oceanic and Atmospheric Administration (NOAA) climate record (NOAA 2021). In the last 20 years, the globe has experienced many extreme events including heatwaves (e.g., Europe 2003; Russia 2010), floods (e.g., USA 2011; India 2015), fires (e.g., Australia 2019, 2020), flash flooding in the Arabian deserts (e.g., Saudi Arabia 2009, 2011), and coastal flooding (e.g., Venice 2019, Mumbai 2021, Karachi 2020), which caused catastrophic situations in these regions (e.g., Almazroui et al. 2016,2018; Philips 2020; Zhang et al. 2020; Herring et al. 2019). Are these events a prelude to what is in store in a warmer world, where more intense and more frequent extremes occur as part of the changing climate? Perhaps this is already evident in 2021, which has seen climate extremes break long-standing records by large margins from east to west and north to south. Antarctica recently calved-off the largest iceberg in the world (Climate and Environment 2021). The deadly recent flooding in central Europe, especially in Germany and Belgium where nearly 200 people lost their lives, surprised the region, and is considered a centennial scale (100-year) extreme event (Samenow 2021; Morris et al. 2021; Cornwall 2021). Parts of the Maritime continent, including Indonesia, faced deadly flooding (df Afonson 2021), as did western India (India monsoon 2021). Recent flooding in eastern and central China (China floods 2021) were, according to Gan and Yeung (2021), stand out events in a 1000 years. Scorching heat waves in Canada and the United States of America (US and Canada heatwave 2021) followed by unusual wildfires, along with heat and fire in the southern Europe and recent fires in Turkey and Greece (Turkey 2021), are likely precursors of what is to be expected in a warmer future world. While attribution studies on those recent extreme events have yet to be completed, previous generations of climate models have long projected strong increases in such extremes. As new cycles of Intergovernmental Panel on Climate Change (IPCC) models become available, it is important to assess their potential to simulate future extreme weather events across the globe. This is what is done in the current study.

The IPCC's Special Report for Managing the Risks of Extreme Events and Disasters to Advance Climate Change Adaptation (SREX) indicated a certainty about the increase in the frequency and magnitude of climate extremes (Seneviratne et al. 2012; IPCC 2012). They report that warm daily temperature extremes, more heavy rainfall episodes, and a decrease in cold extremes during the twenty-first century over several regions of the globe. The occurrence probability of hot extremes and their relationship with rainfall deficits at the global scale was investigated by Mueller and Seneviratne (2012). These extreme events often result in destruction of infrastructure, loss of human lives and livestock as well as damage to natural ecosystems, coastal and land areas (Singh et al. 2021; Batibeniz et al. 2020; Chen et al. 2020). The reliable projections and predictions of extreme events are of great importance for implementing adaptation and mitigation strategies (e.g., Bourdeau-Goulet and Hassanzadeh 2021; Abdullah et al. 2020; Ehsan et al. 2019; Travis 2014; Nõges et al. 2010; Abid et al. 2018), in order to avoid human casualties as well as infrastructure and economic losses of billions of dollars (Smith and Matthews 2015).

Global Climate Models (GCMs) from the Coupled Model Intercomparison Project (CMIP) have been used as a primary tool for examining the past and future changes in the mean and extreme of climate at global and regional scales. A plethora of studies (e.g., Ge et al. 2021; Klutse et al. 2021; Li et al. 2021a; Saeed et al. 2021a, b; Akinsanola et al. 2020; Almazroui 2020; Kim et al. 2020; Rastogi et al. 2020; Srivastava et al. 2020; Wehner et al. 2020; Betts et al. 2018; Diffenbaugh et al. 2017) concluded that under the continuously rising global temperature, catastrophic extreme climatic events are happening with ever greater intensity and frequency across the globe. However, representing the characteristics of climate extremes in the past as well as in projections using multiple GCMs has remained an interesting topic in climate change research (e.g., Chen et al. 2021; Sillmann et al. 2013). For instance, Sillmann et al. (2013) compared the performance of the CMIP phases 3 and 5 (CMIP3 and CMIP5) multi-model ensemble means for temperature and precipitation extremes over different global regions, where not much difference was noted for temperature extremes, while a significant difference was noted for precipitation indices, with the CMIP5 models tending to simulate intense precipitation extremes closer to observations. Recently, Fan et al. (2020) considered a large number of temperature extremes over land regions where they showed that CMIP6 models capture the spatiotemporal variations of the observed temperature extremes well compared to a CMIP5 multi-model ensemble (MME), because of the improved spatial mean and skill of the CMIP6 models relative to CMIP5 models. Generally, there is ample evidence that GCMs exhibit large biases both in temperature and precipitation simulations as compared to observation (e.g., Trenberth 2011), yet it is encouraging to see a gradual improvement in the CMIP models, and that the latest

generation of models is performing better than the earlier ones in simulating climate extremes (Li et al. 2021b; Kim et al. 2020).

The present study aims to evaluate the projected changes in multiple temperature and precipitation extreme indices based on an MME from 21 GCMs that participated in Phase 6 of CMIP over 26 sub-regions, including the entire global landmass over the SREX regions. The CMIP6 models utilize the latest scenarios, namely Shared Socioeconomic Pathways (SSP) (Eyring et al. 2016). Compared with their ancestors (e.g., CMIP3 and CMIP5), the models in the CMIP6 suite are of high resolution (both in space and time) and have comprehensive physical and dynamical schemes enabling the climate research community to tackle a variety of scientific questions related to increasing global warming and its impacts. CMIP6 datasets were also employed to investigate the large-scale picture of the most intense temperature and precipitation extremes by Li et al. (2021b), and a similar regional breakdown over the 41 sub-regions defined for IPCC Sixth Assessment Report (AR6) was conducted by Kim et al. (2020). The present study is complementary to theirs. As climate extremes impact on human and natural systems in different parts of the globe, particularly in recent times, one of the most important tasks is to understand how climate extremes might behave in future periods under different emission scenarios, both globally and for the SREX regions, using CMIP6 multi-model datasets.

2 Data and Methodology

The CMIP6 simulations used are from 21 GCMs (Table 1) for historical (1985–2014) and two future time frames representing mid-century (2036–2065) and end-century (2070–2099) for four SSP scenarios i.e., SSP1-2.6, SSP2-4.5, SSP3-7.0 and SSP5-8.5. Each model was given equal weighting with one ensemble member per model. While some of our results are presented as global maps, we also illustrate the spatial variation and inter-model spread for regions defined in the Special Report on Managing the Risks of Extreme Events and Disasters to Advance Climate Change Adaptation (SREX; Seneviratne et al. 2012; Vogel et al. 2020). All the extreme indices are calculated at each GCM's native resolution as presented in Table1, followed by a regridding to 1°×1° using bi-linear interpolation in order to carry out ensemble-based analyses and statistics. All the indices are calculated for each GCM using daily data.

Among the many available climate indices, we focus our analysis here on just four of them, each representing a measure of extreme weather. To determine hot extremes, we compute the annual hottest day (TXx) by calculating the yearly maximum value of the maximum daily temperature for each grid cell. The heat wave frequency index (HWFI) is

Table 1 Overview of CMIP6 models used in this study, the modeling institutions providing them, country of origin, atmospheric resolution, and the ensemble members employed

No.	CMIP6 model name	Country	Atmospheric Resolution (lon×lat in deg)	Variant label
1	ACCESS-CM2	Australia	1.9°×1.3°	r1i1p1f1
2	ACCESS-ESM1-5	Australia	1.9°×1.2°	r1i1p1f1
3	CanESM5	Canada	2.8°×2.8°	r1i1p1f1
4	CMCC-ESM2	Italy	1.3°×0.9°	r1i1p1f1
5	CNRM-CM6-1	France	1.4°×1.4°	r1i1p1f2
6	CNRM-ESM2-1	France	1.4°×1.4°	r1i1p1f2
7	EC-Earth3	Europe	0.7°×0.7°	r1i1p1f1
8	EC-Earth3-Veg-LR	Europe	1.1°×1.1°	r1i1p1f1
9	EC-Earth3-Veg	Europe	0.7°×0.7°	r1i1p1f1
10	FGOALS-g3	China	2°×2.3°	r1i1p1f1
11	GFDL-ESM4	USA	1.3°×1°	r1i1p1f1
12	INM-CM4-8	Russia	2°×1.5°	r1i1p1f1
13	INM-CM5-0	Russia	2°×1.5°	r1i1p1f1
14	IPSL-CM6A-LR	France	2.5°×1.3°	r1i1p1f1
15	MIROC6	Japan	1.4°×1.4°	r1i1p1f1
16	MPI-ESM1-2-HR	Germany	0.9°×0.9°	r1i1p1f1
17	MPI-ESM1-2-LR	Germany	1.9°×1.9°	r1i1p1f1
18	MRI-ESM2-0	Japan	1.1°×1.1°	r1i1p1f1
19	NorESM2-LM	Norway	2.5°×1.9°	r1i1p1f1
20	NorESM2-MM	Norway	0.9°×1.3°	r1i1p1f1
21	UKESM1-0-LL	UK	1.9°×1.3°	r1i1p1f2

calculated by counting the number of days for each event per year when daily maximum temperature remains higher than the 90th percentile of the historical period continuously for at least six consecutive days. For wet extremes, we compute the maximum five-day precipitation (RX5day) as the maximum sum of precipitation falling during five consecutive days for each year. Similarly for dry extremes, consecutive dry days (CDD) are computed as the maximum number of consecutive days with precipitation less than 1 mm per day for each historical as well as future 30-year time frame.

For future evaluation of all four extreme indices, spatial plots are presented based on criteria of robustness and significance. The robustness of the projected signal is based on the agreement among different model projections on the direction of changes, where the change in the projected signal, whether an increase or decrease, is considered to be robust if at least 66% of the models agree on the direction of change (Haensler et al. 2013). Meanwhile, the significance of the change signal is measured by employing a two-tailed Student's t test based on equal and unequal variance between the future and historical data for each grid box (Kapic et al. 2011). Equal and unequal variance is determined for each grid box using an F test (Archdeacon 1994).
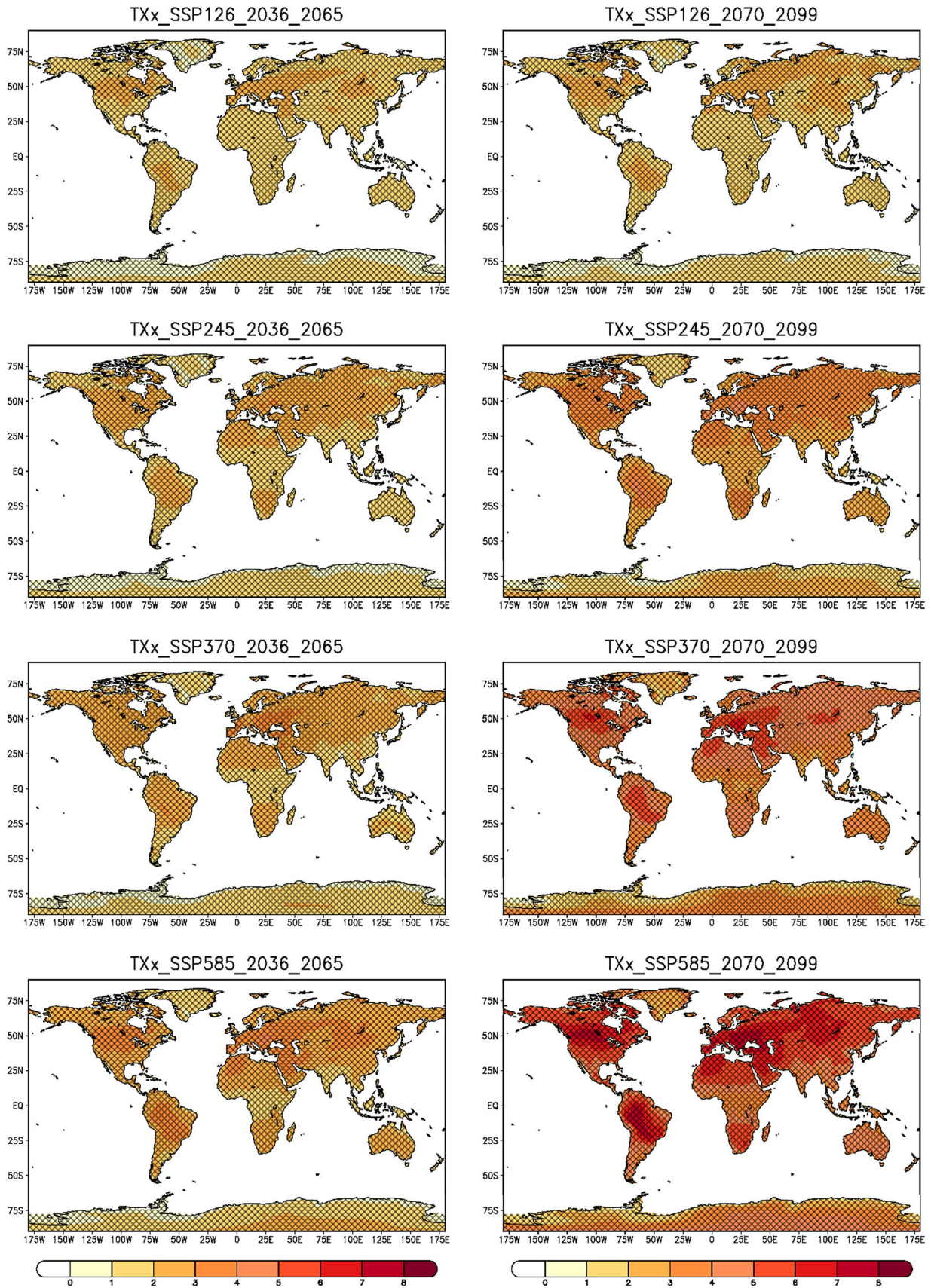
TXx_SSP126_2036_2065

TXx_SSP126_2070_2099

TXx_SSP245_2036_2065

TXx_SSP245_2070_2099

TXx_SSP370_2036_2065

TXx_SSP370_2070_2099

TXx_SSP585_2036_2065

TXx_SSP585_2070_2099

In addition to the spatial plots, changes are presented using box and whisker diagrams representing the spatial variability for each SREX region (see too Vogel et al. 2020). These diagrams are plotted by taking temporal average across all the GCMs for two future time horizons as compared to the reference period for four SSP scenarios, where the boxes and whiskers represent the 66% likely range (17th to 83rd percentile) and very likely range (5th to 95th percentile), respectively. Finally, the temporal distribution across all GCMs for the three-time frames are further analyzed using the kernel density distribution (KDD) over each SREX sub-region. Note that prior to applying KDD, the normal distribution, binomial distribution, and Poisson distribution were applied and found to be not suitable for the data used. The basic theory of KDD can be found in Jones (1990) while the similar but updated kernel density estimation (KDE) is presented by Kamalov (2020). The KDD plots are based on $M \times N$ degrees of freedom, where "M" is the number of Models and "N" is the number of years. Here, regional KDD is generated by first taking the regional average over all land points, and then employing a bandwidth of 0.1 for the data of 30 years across 21 GCMs. To explain it further, we first calculate the spatial average over the region of interest for each CMIP6 model and then concatenated data from all GCMs to make a sample that consisted of 630 values (i.e., $21 \times 30 = 630$, where 21 is the number of models, and each model has 30 values).

3 Results and Discussion

3.1 Projected Changes in Temperature Indices

The temperature extremes in the form of heat waves or cold spells impacts human health, the biophysical environment, ecosystems, and energy consumption (Hales et al. 2003; McGregor et al. 2005; Frank et al. 2015). These extremes occur at various time scales ranging from daily to monthly and annual scales. Many previous studies (e.g., Brown et al. 2008; Christensen et al. 2007; Meehl et al. 2007; Trenberth et al. 2007; Alexander et al. 2006) focused on temperature extremes and the mechanism of changes in these extremes. As mentioned in the previous section, here we examine the

projected changes in the annual hottest day temperature (TXx) and the extreme heat wave frequency (HWFI).

3.2 Projections of Annual Hottest Day Temperature (TXx)

Trends in temperature extremes can sometimes be different for the most extreme temperature cases (e.g., TXx) than for less extreme events (e.g., warm days) (Brown et al. 2008; Alexander et al. 2006). The reason for this is that the moderate extremes e.g., warm days/nights are generally computed for each day with respect to the long-term statistics for that day. Thus, an increase in warm days from annual analyses does not necessarily imply warming for the very warmest days of the year (Seneviratne et al. 2012). Note that the CMIP6 multimodel extreme TXx index is closer to the observations than is the CMIP5 index over most of the globe (Chen et al. 2020; Kim et al. 2020). Freychet et al. (2021) noticed that the best estimate of extremely hot changes by the end of the century could be worse than previously estimated, mostly for tropical and subtropical regions as well as South and East Asia. Therefore, we first examined the projected changes in the annual hottest day temperature over the entire globe and 26 SREX regions (see Figure S1). Figure 1 shows the projected changes in the TXx, which increase significantly over all regions under all future scenarios as compared to the reference period. TXx is projected to increase more over the higher latitudes as compared to the tropical regions. Except for the Amazon region, most of the tropical regions located in Africa and southeast Asia display less increase in TXx values compared to the higher latitudes. This result is in line with Vogel et al. (2020) who analyzed hot extremes using CMIP6 multimodel present day climate along with different levels of additional global warming ($+1$ °C, $+1.5$ °C, $+2$ °C, and $+3$ °C). The projected increase in TXx scales linearly with the future increase in the concentration of greenhouse gases. Figure 1 shows substantial increase in TXx over the Mediterranean region and adjacent parts of Europe and Central Europe, Northern Africa, and Arabian Peninsula. The projected patterns of TXx are consistent among all future scenarios, and also with the results of the CMIP5 analysis reported by Seneviratne and Hauser (2020). The projected changes in the TXx are more pronounced at the end-century as compared to the mid-century. These changes are more intense in the case of the high emission SSP5-8.5 scenario. The projected changes in TXx are robust over global land areas as the majority of CMIP6 models agree with the sign of change.

The spatial variation of the projected TXx over global land and its 26 SREX regions is shown in Fig. 2. The projected change in the median values of TXx over all the SREX regions increases linearly with an increase in the greenhouse gases for the mid- and end-century.
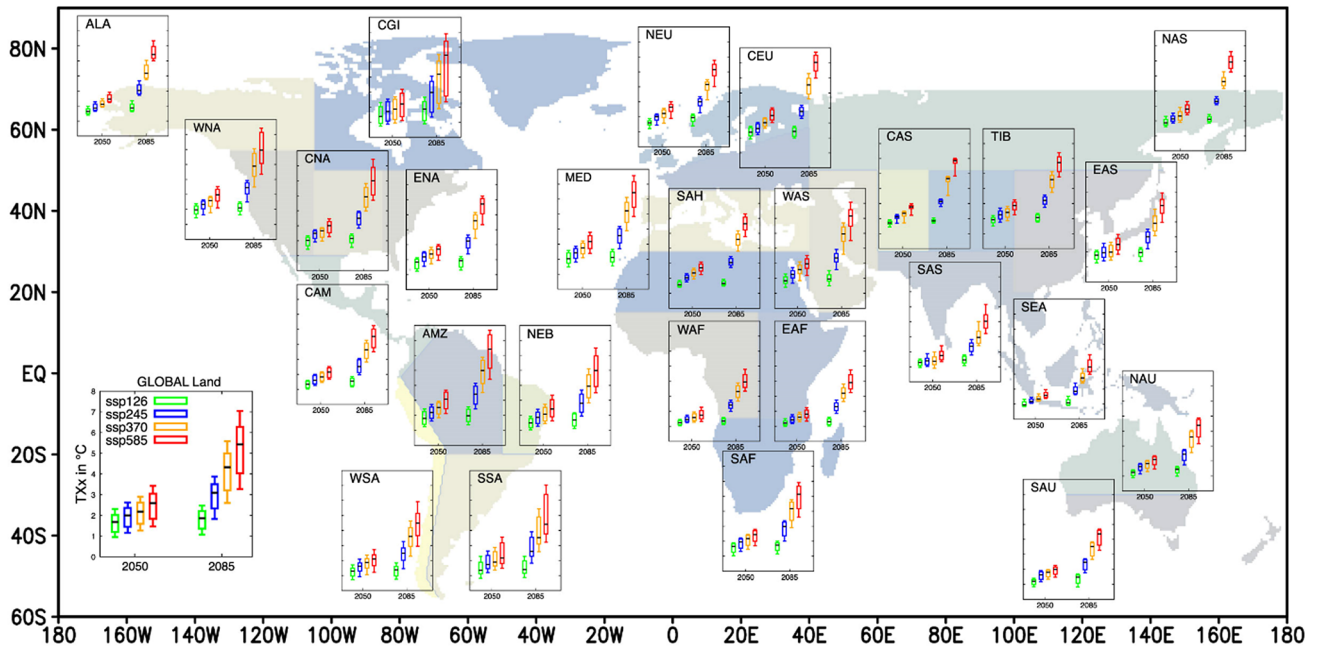
Fig. 2 Projected changes (in °C) in TXx. The box-whisker plots (see legend for more information) show the spatial variability obtained by taking temporal average across all the GCMs for two time horizons, 2036 to 2065 and 2070 to 2099, as compared to the reference period (1985–2014), and for four SSP scenarios (SSP1-2.6, SSP2-4.5, SSP3-7.0 and SSP5-8.5). Results are based on 21 CMIP6 GCMs contributing to the CMIP6. See Figure S1 for the definition of The 26 SREX regions are: Alaska/NW Canada (ALA), Eastern Canada/Greenland/Iceland (CGI), Western North America (WNA), Central North America (CNA), Eastern North America (ENA), Central America/Mexico (CAM), Amazon (AMZ), NE Brazil (NEB), West Coast South America (WSA), South- Eastern South America (SSA), Northern Europe (NEU), Central Europe (CEU), Southern Europe/the Mediterranean (MED), Sahara (SAH), Western Africa (WAF), Eastern Africa (EAF), Southern Africa (SAF), Northern Asia (NAS), Western Asia (WAS), Central Asia (CAS), Tibetan Plateau (TIB), Eastern Asia (EAS), Southern Asia (SAS), Southeast Asia (SEA), Northern Australia (NAS) and Southern Australia/New Zealand (SAU). Values are computed for land points only. The 'Global' analysis (inset box) displays the change in TXx using all land grid points
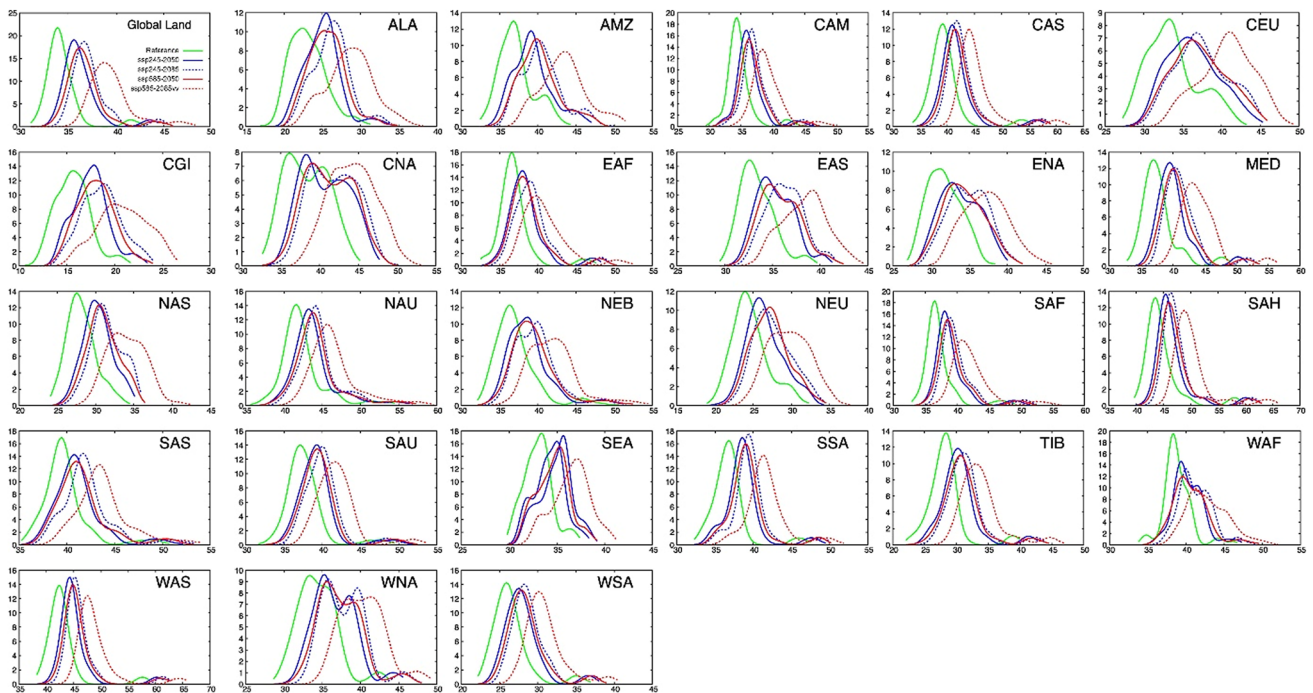

Fig. 3 Kernel density distribution of annual values of TXx over each SREX region in the future periods under all four scenarios. Each regional distribution has been generated by first taking the regional average over all land point, and then employing a bandwidth of 0.1 for the data of 30 years across 21 CMIP6 GCMs. Horizontal axis represents values of temperature (in °C). The scales along x- and y-axis are not same for all panels
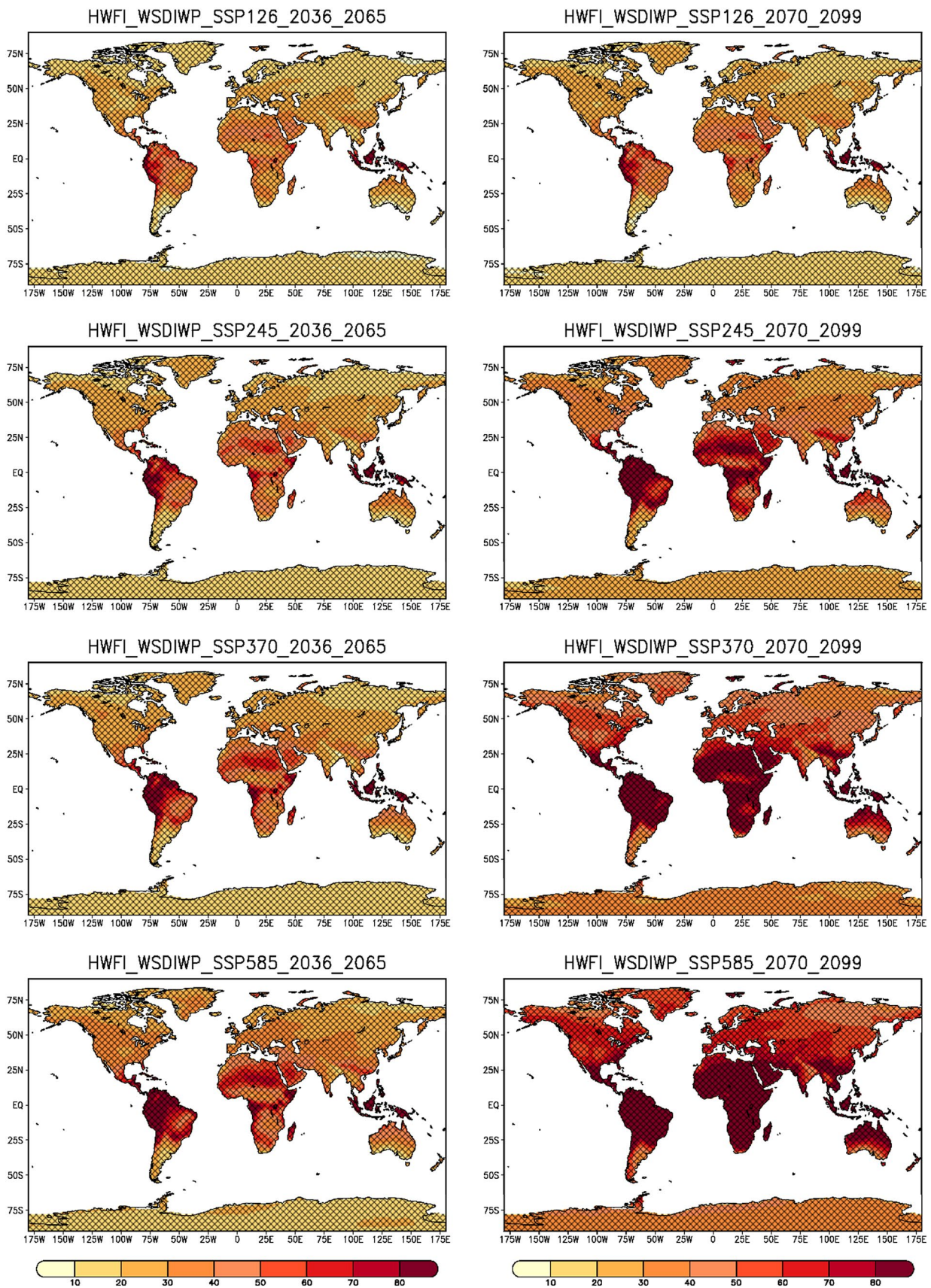
Fig. 4 Same as Fig. 1, but for HWFI (in number of days)

The globally averaged TXx is projected to increase by 1.5–2.5 °C by mid-century, and by 2–5.5 °C by the end of the century under the four emission scenarios. The projected TXx reveals smallest spatial variability under SSP1-2.6 and largest under the high emission scenario SSP5-8.5. The spatial variability increases towards the end of the twenty-first century as compared to the near future period. The projected spatial variability in the TXx displays marked regional differences. With some exceptions, such as the Amazon and Northeastern Brazil, most of the tropical regions show small spatial variability as compared to the mid and high latitudes. Moreover, the TXx projections for the end-century show significant differences between different SSP scenarios. For example, the TXx displays an increase in median value of 2.5 and 7 °C under SSP1-2.6 and SSP5-8.5, respectively, over the CEU region. Interestingly, for all SREX regions, the difference in the projected TXx signals for mid- and end-century is negligible for the SSP1-2.6, which can be attributed to its peaked emission/concentration pathway during the twenty-first century. For other future scenarios (e.g., SSP2-4.5, SSP3-7.0, and SSP5-8.5), the TXx is projected to increase more by the end-century as compared to the mid-century.

The KDD curves show a shift in the TXx distribution to the right side for the future periods under SSP2-4.5 and SSP5-8.5 scenarios as compared to the reference period (Fig. 3). The TXx distributions over SREX regions CAM, CAS, EAF, WAS, and WSA show a similar pattern for future periods as noticed in the reference period. Some other regions (e.g., AMZ, CEU, CGI,

ENA, NAS etc.) display flatter distributions in the future period as compared to the reference period. The CMIP6 models over some regions (e.g., CNA, WNA) display double peaks in the TXx distribution in the reference period as well as in the future period, except for SSP5-8.5 for the end-century, where this behavior (i.e., two peaks) disappears. In some regions, the CMIP6 models display a drastic increase in TXx as compared to the reference period. For example, SAH and WAS are regions where CMIP6 models, towards their tails, simulate TXx values up to 65 °C in the future under SSP5-8.5. The CMIP6 models in the Amazon region show the highest value of TXx up to 45 °C in the reference period; whereas, in the future it may reach 50 °C under high emission scenarios. In many regions, based on the CMIP6 models, the tails of the distributions show values exceeding 50 °C in the future. The above discussion reveals that extremely hot days will become even hotter in the future period over almost all regions in the world, while the largest increase is likely over the Mediterranean and adjacent European regions, North America, the Amazon, and South Africa.

3.3 Extreme Heat Wave Days (HWFI)

Figure 4 shows the spatial distribution of HWFI for mid- and end-century. Contrary to the TXx, the HWFI increases more in the tropical regions as compared to the higher latitudes. Again, there is a linear increase in the heat wave days with increasing greenhouse gas
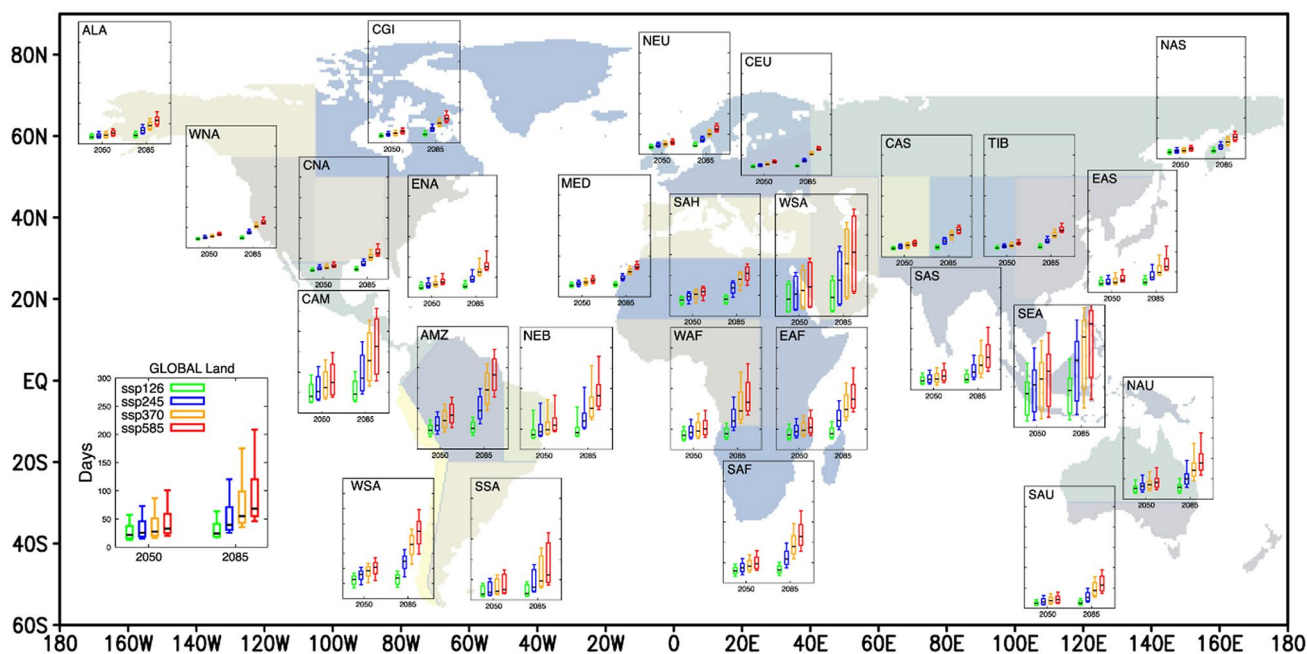

Fig. 5 Same as Fig. 2, but for HWFI (in number of days)

concentrations in the future period. As expected, the lowest increase in the HWFI is noticed under SSP1-2.6, while the highest increase occurs under SSP5-8.5. Moreover, the projections show a larger increase in the heat wave days towards the end of the twenty-first century as compared to the reference period. By the end of the twenty-first century, a large part of the globe shows a drastic increase in heat waves under the high emission scenario SSP5-8.5. The largest increase in the HWFI is projected over the Amazon, Sahara, tropical and southern parts of Africa, Arabian Peninsula, south and southeast Asia, and northern Australia. Interestingly, the projections show more spatial variability in the southern hemisphere as compared to the northern hemisphere. The projected HWFI shows enhanced variability in tropical regions such as CAM, AMZ NEB, WAF and SEA (Fig. 5). The largest increase in the projected spatial variability of HWFI occurs over the SEA region where some grid cells show an increase of more than 300 days under the high emission scenario as compared to the reference period. Globally, the spatial variability also increases towards the end of the century. The HWFI is projected to increase from 50 to 200 days as compared to the reference period, under the high emission scenario SSP5-8.5 (Fig. 5).

KDD plots indicate that future periods are skewed right and become flatter under all scenarios as compared to the reference period (Fig. 6). The distribution of HWFI in future periods reveals a clear increase in the number of heat wave days in the twenty-first century as compared to the reference period under all scenarios over all SREX regions. This increase is more pronounced for the end-century as compared to mid-century and the reference period. By the end of the twenty-first century, the right tail of the distribution is flatter under SSP5-8.5 in some regions (e.g., AMZ, CGI, EAF, NEB, SAF, SAU, SSA, WAF), suggesting a highly pronounced increase in HWFI compared to the reference period. In most regions, the CMIP6 models simulate an increase of more than 100% in the heat wave days under SSP5-8.5 for the end-century period. For example, in the AMZ region, the KDD curve shows a maximum of 150 heat wave days in the reference period, but this number increases to 350 days under SSP5-8.5 for the end-century (Fig. 6). In some regions (e.g., EAF, NEB, SAF, SSA, WAF etc.) the future projections reveal an increase of more than 200% in the heatwave days as compared to the reference period. The results indicate a clear increase in the heat wave days at global and regional scales. However, their frequency and intensity vary regionally.

4 Projected Changes in Precipitation Indices

4.1 Consecutive 5 days Precipitation (RX5day)

Consecutive precipitation amplification may increase the risk of heavy flooding, imposing heavy costs to socio-economic sectors. Excessive precipitation can lead to heavy floods that may also degrade water quality, harming human
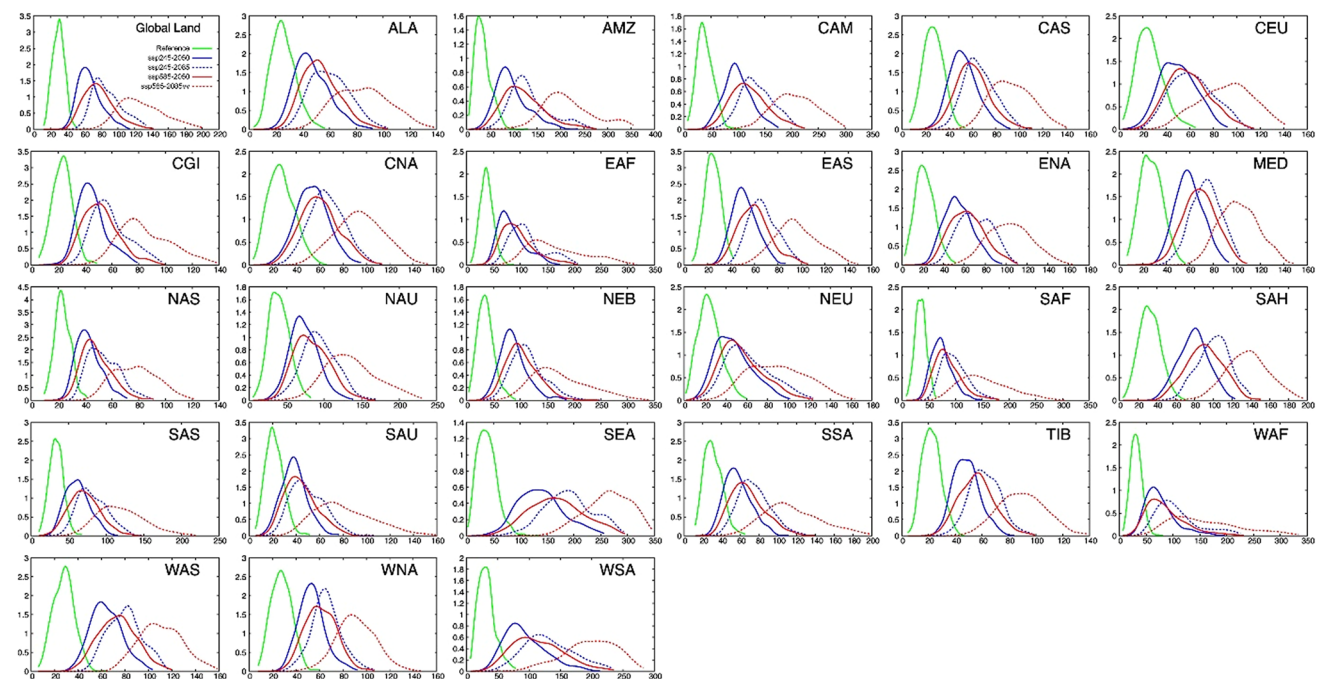

Fig. 6 Same as Fig. 3, but for HWFI (in number of days) where horizontal axis represents values of HWFI (in number of days). The scales along x- and y-axis are not same for all panels
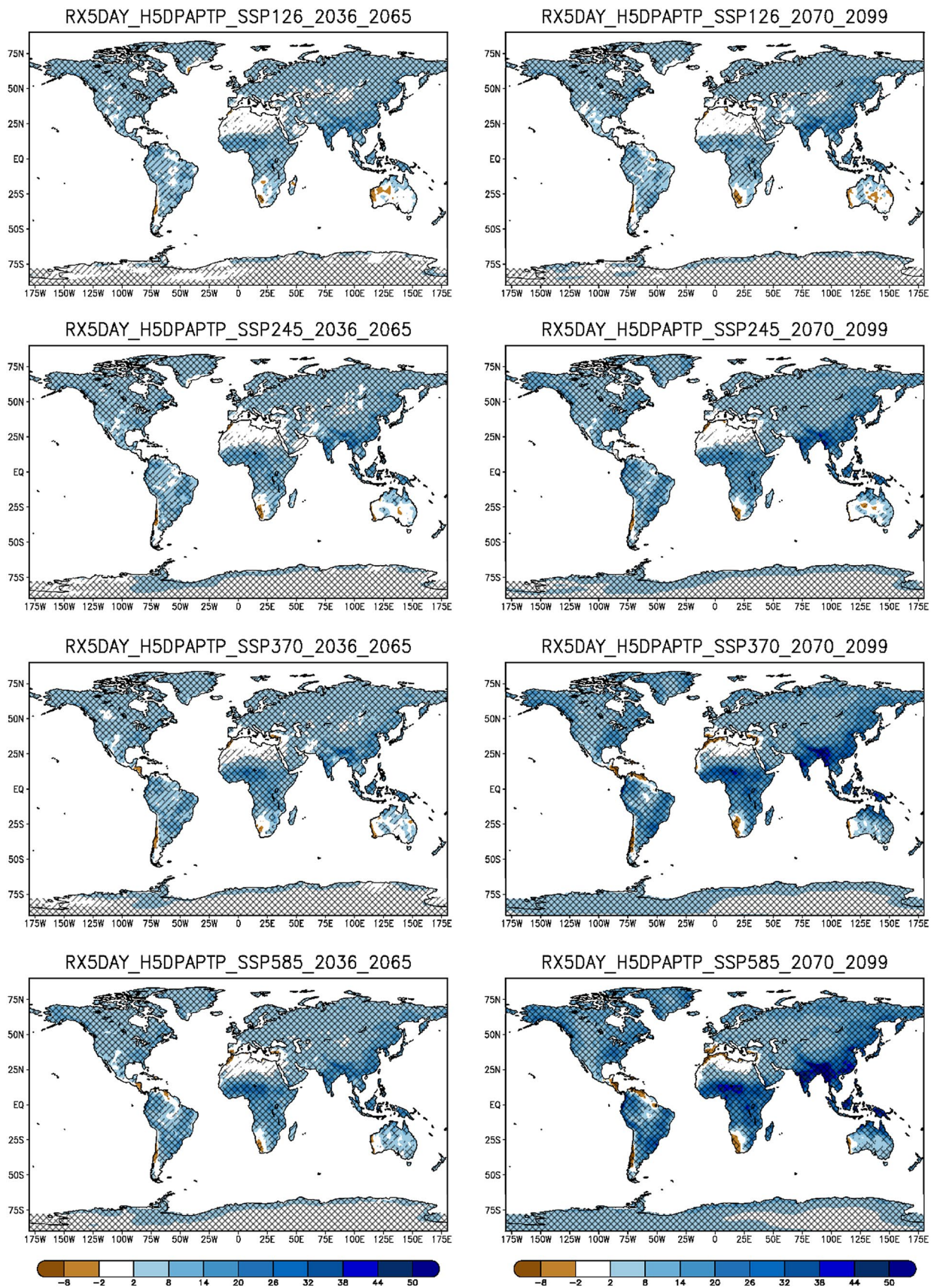
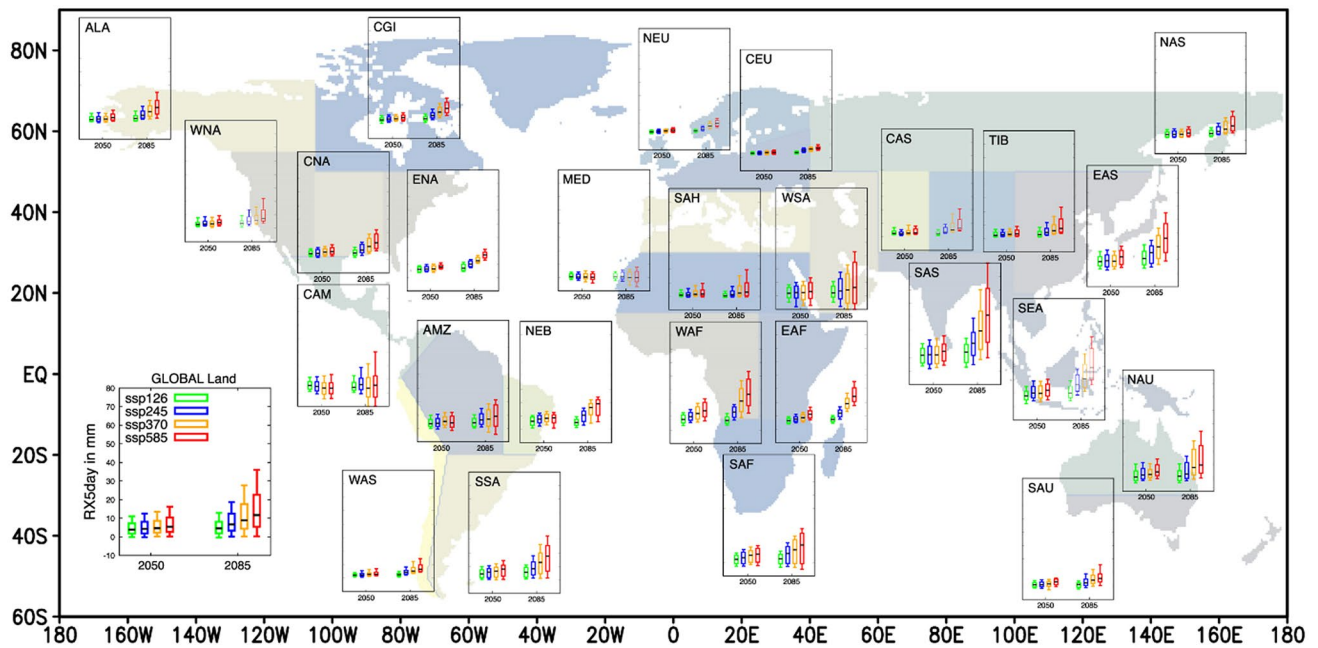**Fig. 7** Same as Fig. 1, but for RX5day (in mm)

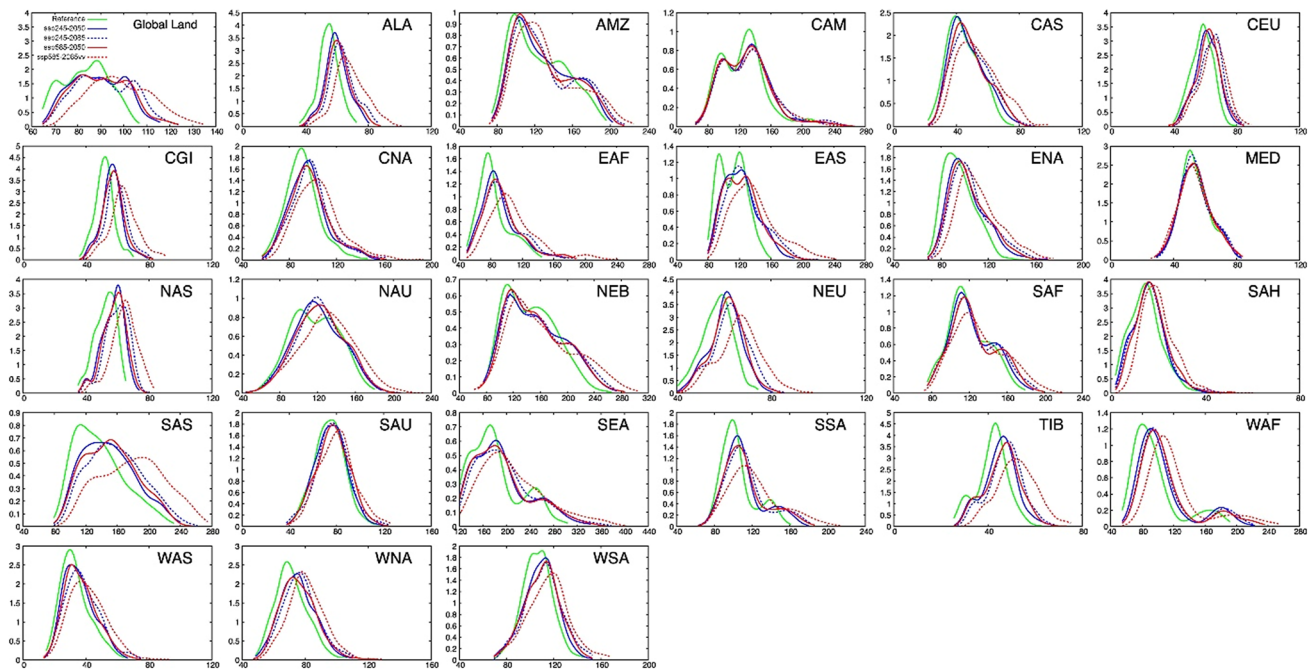**Fig. 8** Same as Fig. 2, but for RX5day (in mm)

Fig. 9 Same as Fig. 3, but for RX5day where horizontal axis represents values of RX5day (in mm). The scales along x- and y-axis are not same for all panels

health and ecosystems (Marengo et al. 2020a, b). In addition to flooding, extreme consecutive precipitation also increases the risk of landslides (Marengo et al. 2020a, b). Above-normal consecutive precipitation raises the water table and saturates the ground; hence slopes can lose their

stability, causing a landslide. We therefore examined the projected changes in annual maximum consecutive 5-day precipitation (RX5day) under different SSP scenarios (Fig. 7). Note that RX5day is reasonably well reproduced by CMIP6 as compared to the observations, in line with
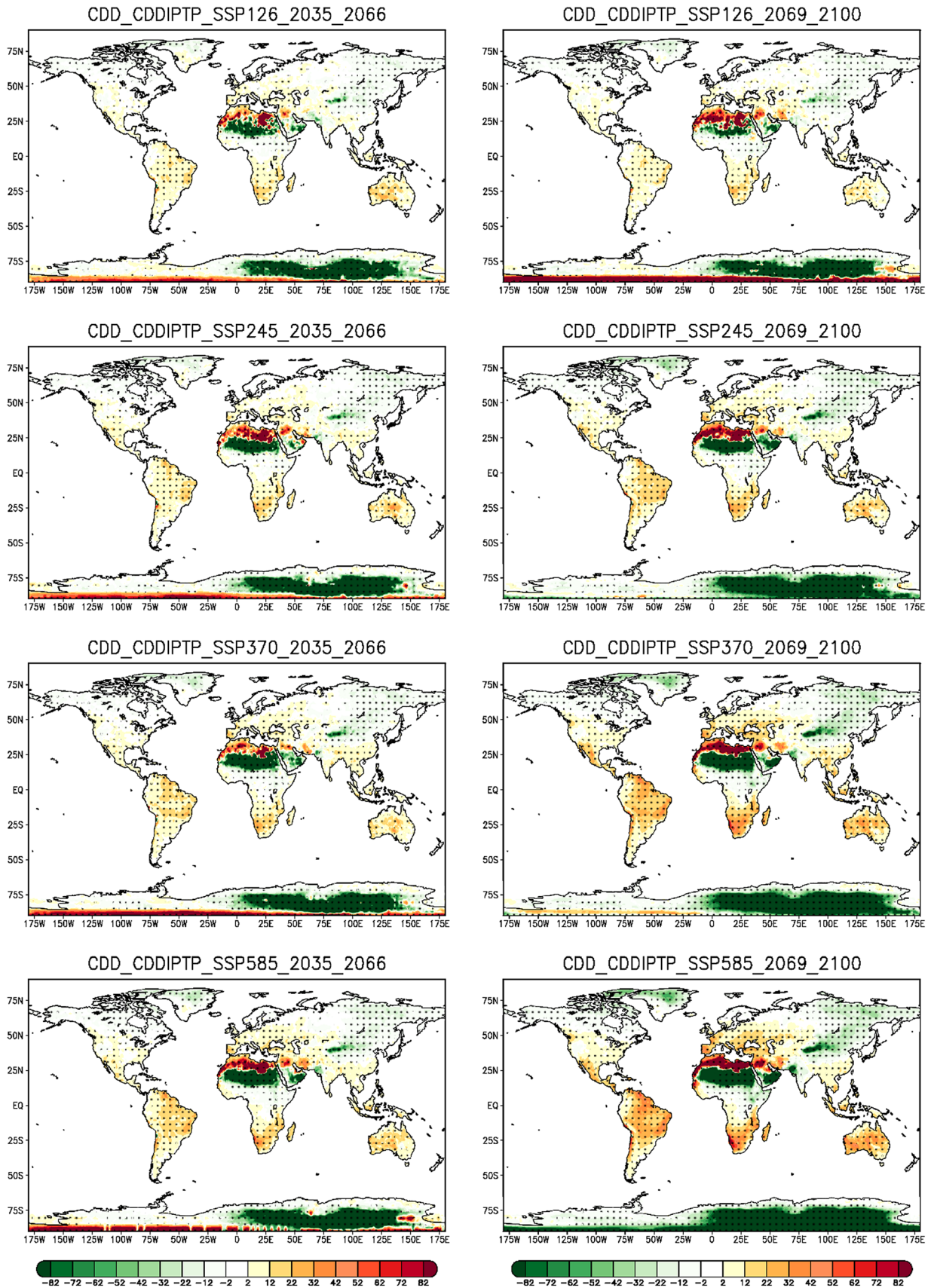
Spatial distribution of future changes (in number of days) in the longest streak of consecutive dry days (CDD) in the two future time slices (2036–2065 and 2070–2099) as compared with the reference period (1985–2014) for scenarios (SSP1-2.6, SSP2-4.5, SSP3-7.0 and SSP5-8.5). The dots represent the grid boxes showing robust change which is defined when 66% of all models project a climate change signal in the same direction

the CMIP5 result (Chen et al. 2020). However, in the precipitation extreme indices climatology patterns, a substantial reduction of dry bias was noticed over South Asia, South America, and east Asia in CMIP6 as compared with CMIP5 (Kim et al. 2020).

The RX5day is projected to increase significantly over most of the globe. Some regions, such as northern Africa and adjacent parts of Mediterranean, western Arabian Peninsula, Caribbean, northeastern and southwestern strips of South America, South Africa, and large areas in Australia show either no change or a reduction in RX5day as compared to the reference period. The RX5day is projected to increase more in tropical Africa, South Asia, East Asia, and Southeast Asia as compared to other regions in the world (Figs. 7, 8). The SAS, EAS and SEA climates are strongly affected by the monsoon regime. Future projections of monsoon rainfall from CMIP3 to CMIP6 models show an intensification over the Asian region with a corresponding increase in precipitation extremes, which has many implications for socioeconomic sectors in these regions (Ge et al. 2021; Almazroui et al. 2020a; Grose et al. 2020; Narsey et al. 2020; Scoccimarro and Gualdi 2020; Zhou et al. 2014). Like other indices, the projected changes in RX5day precipitation intensify with future increases in the concentration of greenhouse gases over all SREX regions except Australia where negative change over central parts disappear in the case of high emission scenarios. The projected changes are more significant under higher emissions than under lower emission scenarios. The projected spatial variability of RX5day is shown in Fig. 8. The tropical regions display large spatial variability of RX5day as compared to the higher latitudes. Further, the RX5day exhibits large spatial variability in the southern hemisphere as compared to the northern hemisphere. Moreover, the spatial variability in RX5day increases with increasing greenhouse gas concentrations. Spatial variability is projected to increase more under the high emission scenario SSP5-8.5 by the end of the twenty-first century. The largest spatial variability in RX5day is projected over the SAS region, where some grid-cells may receive over 80 mm more than the reference period. The large spatial variability in RX5day could be related to enhanced land surface heterogeneity and the occurrence of monsoons. The KDD of RX5day displays nearly the same pattern over most of the SREX regions during present and future periods (Fig. 9). However, the SAS region

is an exception where the distributions are skewed right for both future periods and scenarios. This further indicates the SAS region is more prone to extreme floods in future under high emission scenarios.

4.2 Consecutive Dry Days (CDD)

Similar to heavy floods, persistent drought-like conditions severely impact various sectors of life by influencing agriculture, vegetation, and groundwater levels. Therefore, we further examined the projected changes in the longest streak of consecutive dry days (CDD) (Fig. 10) in the two future time slices (2035–2065 and 2069–2100) as compared with the reference period (1985–2014) for scenarios SSP1-2.6, SSP2-4.5, SSP3-7.0 and SSP5-8.5. The future simulations project an intensification of CDD, with increases over the Mediterranean and adjacent areas of northern Africa and Europe, northwestern Arabian Peninsula, South America, South Africa, and Australia. Decreases are projected over Sahara, southern Arabian Peninsula, Greenland, and northeastern parts of Russia. The Mediterranean region is the climate change hotspot (Giorgi 2006), where south of the Mediterranean the largest increase is noted (more than 80 days as compared to the reference period's episode), while over the European region it reaches up to 30 days, which indicates that more prolonged episodes of droughts may occur over this region in the future. South Africa is another region prone to droughts (Pascale et al. 2020). The Cape Town region in South Africa recently experienced a severe multiyear drought with strong rainfall anomalies (Sousa et al. 2018; Mahlalela et al. 2019). The CMIP6 multi-model mean climate projections also show strong dryness over South Africa (Almazroui et al. 2020b). The projected increase in the CDD over South Africa indicates prolongation of future drought-like conditions over South Africa, including Cape Town. Overall, the hotspot regions for increased hot and dry events are projected to be over the Amazon and Brazil, the Mediterranean, Southern Africa, and parts of Australia. These are in line with the hotspot regions mentioned in Vogel et al. (2020), who used CMIP6 present-day climate and different levels of additional global warming. They also mentioned as hotspots the Sahel region and Indonesia under +1.5 °C global warming, along with the Andes and Himalayan for +2.0 °C global warming.

The CDD projections also display strong spatial variability over global land and 26 SREX regions (Fig. 11). CMIP6 models tend to overestimate the CDD over some regions of Africa (e.g., northeast Africa, central east Africa) and South America (e.g., south Amazonia, north South America, northeast South America). However, they underestimate the CDD over Sahara, Southwest Africa, and the Tibetan-Plateau (Kim et al. 2020). In addition, they stated that CMIP6 based CDD is larger than CMIP5 CDD over some African
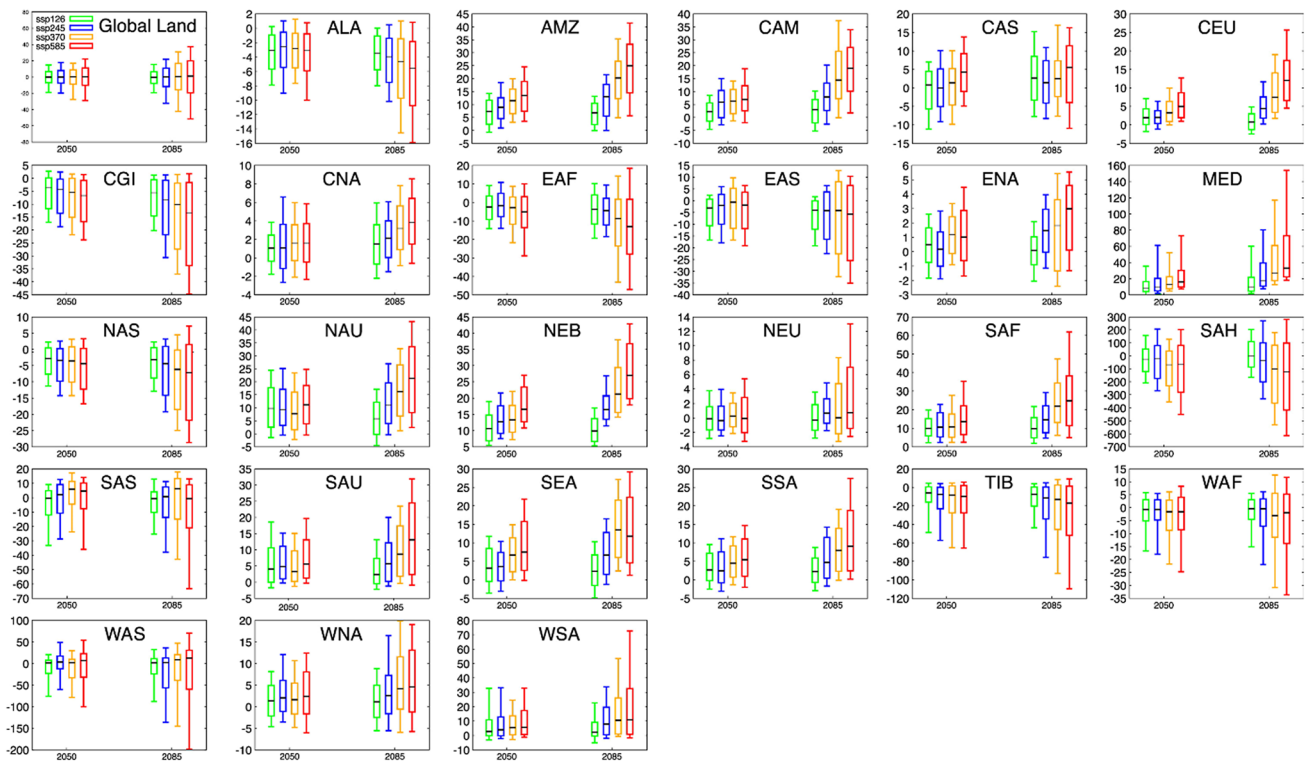
Fig. 11 Same as Fig. 2, but for CDD. Unlike Fig. 2, the results are presented in separate panels for better depiction

sub-regions. The projected CDD spatial variability increases more by the end-century as compared to mid-century. Moreover, the projected variability is higher under the high emission scenario. For the low emission scenario SSP1-2.6, the projected changes in the median values of CDD are nearly the same for mid- and end-century with respect to the reference period. Furthermore, the spatial variability of CDD does not show any remarkable difference between mid- and end-century periods. The above results indicate that the increase in future extreme events can be minimized by limiting the global greenhouse emissions according to the Paris Agreement.

5 Summary and Conclusions

In this study, we examined projected change in hot and wet extreme events that occur once in a year using a 21-member CMIP6 multi-model daily dataset. The projected changes are analyzed by using four indices for mid-century (2036–2065) and end-century (2070–2099) with respect to the reference period (1985–2014) under four emission scenarios (SSP1-2.6, SSP2-4.5, SSP3-7.0, and SSP5-8.5) for the entire global land and 26 SREX regions. The results indicate a significant

and robust increase of hot temperature and precipitation extremes over most of the land areas. Our results show that the annual hottest day temperature (annual maximum of maximum daily temperature) increases more in the extratropical regions as compared to the tropical areas, while the frequency of extreme heat wave days is projected to increase more in the tropical regions. Consecutive dry days (CDD) are projected to increase more in the Amazon and Brazil, Mediterranean, South Africa, and Australia (see Fig. 10). In general, the hotspot regions for increased hot and dry events are projected over Amazon and Brazil, Mediterranean, Southern Africa and parts of Australia.

On the other hand, the Asian monsoon regions (e.g., South Asia, East Asia, and Southeast Asia) are more prone to extreme flooding, associated with the projected increase in the annual maximum consecutive 5-day precipitation. The projected changes in extremes display large spatial variability within each SREX region. The spatial variability increases with increasing greenhouse gas concentration, and it is highest at the end-century as compared to the mid-century and reference period. As expected, there is no remarkable change in extremes and their spatial variability under the low emission scenario SSP1-2.6.

The results indicate that increased concentration of global greenhouse gases leads to substantial increases in the extreme events and their intensities. This is recently evident in the deadly heatwave in the US and Canada in June 2021, where temperatures rose above 49.6 °C in Lytton, British Columbia, indicating that human-caused climate disruption is making extreme weather even worse than predicted (Schiermeier 2021) and that societies must be prepared for more such events in future. Our results further underline that for some extremes (e.g., RX5day and HWFI), the countries of the global south already having high incidence of poverty, will be at disproportionately higher risk. The lowest emission scenario, SSP1-2.6 in our analysis, is projected to take the world to almost 2 °C above pre-industrial levels by the end-century. Lower increases in extremes for SSP1-2.6 analyzed in our study, highlight the importance of stronger mitigation actions to stabilize the global temperature at 1.5 °C in-line with the Paris Agreement goals. The findings of the present study indicate that a stabilization of CO_2 emissions consistent with the aims of the Paris Agreement would substantially reduce the risk of increase in extreme events.

Compliance with ethical standards

Conflict of Interest The authors have no conflict of interest.

References

Abdullah AYM, Bhuian MH, Kiselev G et al (2020) Extreme temperature and rainfall events in Bangladesh: a comparison between coastal and inland areas. Int J Climatol. https://doi.org/10.1002/joc.6911

Abid M, Almazroui M, Kucharski F et al (2018) ENSO relationship to summer rainfall variability and its potential predictability over Arabian Peninsula region. Clim Atmos Sci 1:20171. https://doi.org/10.1038/s41612-017-0003-7

Akinsanola AA, Kooperman GJ, Pendergrass AG, Hannah WM, Reed KA (2020) Seasonal representation of extreme precipitation indices over the United States in CMIP6 present-day simulations. Environ Res Lett. https://doi.org/10.1088/1748-9326/ab92c1

Alexander LV, Zhang X, Peterson TC et al (2006) Global observed changes in daily climate extremes of temperature and precipitation. J Geophys Res Atmos 111:D05109. https://doi.org/10.1029/2005JD006290

Almazroui M, Kami S, Ammar K, Keay K, Alamoudi AO (2016) Climatology of the 500-hPa Mediterranean storms associated with Saudi Arabia wet season precipitation. Clim Dyn 47(9):3029–3042

Almazroui M, Raju PVS, Yousef A et al (2018) Simulation of extreme rainfall event of November 2009 over Jeddah, Saudi Arabia: the explicit role of topography and surface heating. Theor Appl Climatol 132:89–101. https://doi.org/10.1007/s00704-017-2080-2

Almazroui M, Saeed S, Saeed F et al (2020a) Projections of precipitation and temperature over the South Asian Countries in CMIP6. Earth Syst Environ 4:297–320. https://doi.org/10.1007/s41748-020-00157-7

Almazroui M, Saeed F, Saeed S et al (2020b) Projected change in temperature and precipitation over Africa from CMIP6. Earth Syst Environ 4:455–475. https://doi.org/10.1007/s41748-020-00161-x

Almazroui M (2020) Changes in temperature trends and extremes over Saudi Arabia for the period 1978–2019. Adv Meteorol 2020:21. https://doi.org/10.1155/2020/882842

Archdeacon T (1994) Correlation and regression analysis: a historian's guide, 1st edn. University of Wisconsin Press, Madison, Wisconsin, USA

Batibeniz F, Ashfaq M, Diffenbaugh NS et al (2020) Doubling of U.S. population exposure to climate extremes by 2050. Earth Future. https://doi.org/10.1029/2019EF001421

Betts RA, Lorenzo A, Catherine B et al (2018) Changes in climate extremes, fresh water availability and vulnerability to food insecurity projected at 1.5°C and 2°C global warming with a higher-resolution global climate model. Trans R Soc A. https://doi.org/10.1098/rsta.2016.0452

Bourdeau-Goulet S-C, Hassanzadeh E (2021) Comparisons between CMIP5 and CMIP6 models: simulations of climate indices influencing food security, infrastructure resilience, and human health in Canada. Earth Future. https://doi.org/10.1029/2021EF001995

Brown SJ, Caesar J, Ferro CAT (2008) Global changes in extreme daily temperature since 1950. J Geophys Res Atmos 113:D05115. https://doi.org/10.1029/2006JD008091

Chen CA, Hsu H-H, Liang H-C (2021) Evaluation and comparison of CMIP6 and CMIP5 model performance in simulating the seasonal extreme precipitation in the Western North Pacific and East Asia. Weather Clim Extrem. https://doi.org/10.1016/j.wace.2021.100303

Chen H, Sun J, Lin W, Xu H (2020) Comparison of CMIP6 and CMIP5 models in simulating climate extremes. Sci Bull 65:1415–1418. https://doi.org/10.1016/j.scib.2020.05.015

China floods (2021c) China floods: 12 dead in Zhengzhou train and thousands evacuated in Henan. Accessed 5 Aug 2021. https://www.bbc.com/news/world-asia-china-57861067

Christensen JH, Hewitson B, Busuioc A et al (2007) Regional climate projections. In: Solomon S, Qin D, Manning M, Chen Z, Marquis M, Averyt KB, Tignor M, Miller HL (eds) Climate change 2007: the physical science basis. Contribution of Working Group I to the Fourth Assessment Report of the Intergovernmental Panel on climate change. Cambridge University Press, Cambridge, UK, pp 847–940

Climate and Environment (2021) Iceberg splits from Antarctica, becoming World's largest. Accessed 5 Aug 2021. https://www.nytimes.com/2021/05/20/world/iceberg-antarctica-ronne-a76.html

Cornwall W (2021) Europe's deadly floods leave scientists stunned. Clim Europe. https://www.sciencemag.org/news/2021/07/europe-s-deadly-floods-leave-scientists-stunned. https://doi.org/10.1126/science.abl5271

df Afonson J (2021) Floods and landslides in Indonesia and East Timor kill more than 100. Accessed 5 Aug 2021. https://www.bbc.com/news/world-asia-56635297

Diffenbaugh NS, Singh D, Mankin JS et al (2017) Quantifying the influence of global warming on unprecedented extreme climate events. PNAS 114(19):4881–4886

Ehsan MA, Kucharski F, Almazroui M, Ismail M, Tippett MK (2019) Potential predictability of Arabian Peninsula summer surface air temperature in the North American multimodel ensemble. Clim Dyn. https://doi.org/10.1007/s00382-019-04784-3

Eyring V, Bony S, Meehl GA et al (2016) Overview of the coupled model intercomparison project phase 6 (CMIP6) experimental design and organization. Geosci Model Dev 9:937–1958

Fan Xn, Miao C, Duan Q, Shen C, Wu Y (2020) The performance of CMIP6 versus CMIP5 in simulating temperature extremes over the global land surface. J Geophys Res Atmos 125(18). https://doi.org/10.1029/2020JD033031

Frank D, Reichstein M, Bahn M et al (2015) Effects of climate extremes on the terrestrial carbon cycle: concepts, processes and potential future impacts. Glob Chang Biol 21(8):2861–2880. https://doi.org/10.1111/gcb.12916

Freychet N, Hegerl G, Mitchell D et al (2021) Future changes in the frequency of temperature extremes may be underestimated in tropical and subtropical regions. Commun Earth Environ 2:28. https://doi.org/10.1038/s43247-021-00094-x

Gan N, Yeung J (2021) Once in a thousand years' rains devastated central China, but there is little talk of climate change. Accessed 5 Aug 2021. https://edition.cnn.com/2021/07/23/china/china-flood-climate-change-mic-intl-hnk/index.html

Ge F, Zhu S, Luo H, Zhi X, Wang H (2021) Future changes in precipitation extremes over Southeast Asia: insights from CMIP6 multi-model ensemble. Environ Res Lett 16:024013

Giorgi F (2006) Climate change hot-spots. Geophys Res Lett 33:L08707

Grose MR, Narsey S, Delage FP et al (2020) Insights from CMIP6 for Australia's future climate. Earth Future. https://doi.org/10.1029/2019EF001469

Haensler A, Saeed F, Jacob D (2013) Assessing the robustness of projected precipitation changes over central Africa on the basis of a multitude of global and regional climate projections. Clim Change 121:349–363. https://doi.org/10.1007/s10584-013-0863-8

Hales S, Edwards SJ, Kovats RS (2003) Impacts on health of climate extremes. In: Climate change and human health: risks and responses, pp 79–102. https://www.who.int/globalchange/publications/climatechangechap5.pdf

Herring SC, Christidis N, Hoell A, Hoerling MP, Stott PA (2021) Explaining extreme events of 2019 from a climate perspective. Bull Am Meteorol Soc 102(1):S1–S112. https://doi.org/10.1175/BAMS-ExplainingExtremeEvents2019.1

India monsoon (2021b) India monsoon: rescuers search for survivors after heavy rains. Accessed 5 Aug 2021. https://www.bbc.com/news/world-asia-india-57952521

IPCC (2012) Managing the risks of extreme events and disasters to advance climate change adaptation: a special report of working groups I and II of the intergovernmental panel on climate change. Cambridge University Press, Cambridge

Jones MC (1990) The performance of kernel density functions in kernel distribution function estimation. Stat Prob Lett 9(2):129–132

Kamalov F (2020) Kernel density estimation based sampling for imbalanced class distribution. Inf Sci 512:1192–1201. https://doi.org/10.1016/j.ins.2019.10.017

Kapic D, Hlupić N, Lovrić M (2011) Student's t-tests. In: Lovric M (eds) International encyclopedia of statistical science. Springer, Berlin. https://doi.org/10.1007/978-3-642-04898-2_641

Kim YH, Min SK, Zhang X, Sillmann J, Sandstad M (2020) Evaluation of the CMIP6 multi-model ensemble for climate extreme indices. Weather Clim Extrem 29:100269. https://doi.org/10.1016/j.wace.2020.100269

Klutse NAB, Quagraine KA, Nkrumah F, Quagraine KT, Berkoh-Oforiwaa R, Dzrobi JF, Sylla MB (2021) The climatic analysis of summer monsoon extreme precipitation events over West Africa in CMIP6 simulations. Earth Syst Environ 5:25–41. https://doi.org/10.1007/s41748-021-00203-y

Li W, Zhao S, Chen Y et al (2021a) State of China's climate in 2020. Atmos Ocean Sci Lett 14(4):100048. https://doi.org/10.1016/j.aosl.2021.100048

Li C, Zwiers F, Zhang X, Li G, Sun Y, Wehner M (2021b) Changes in annual extremes of daily temperature and precipitation in CMIP6 models. J Clim 34:3441–3460. https://doi.org/10.1175/JCLI-D-19-1013.1

Mahlalela PT, Blamey RC, Reason CJC (2019) Mechanisms behind early winter rainfall variability in the southwestern Cape, South Africa. Clim Dyn 53:21–39. https://doi.org/10.1007/s00382-018-4571-y

Marengo JA, Ambrizzi T, Alves LM et al (2020a) Changing trends in rainfall extremes in the metropolitan area of São Paulo: causes and impacts. Front Clim 2:3. https://doi.org/10.3389/fclim.2020.00003

Marengo J, Alves L, Ambrizzi T et al (2020b) Trends in extreme rainfall and hydrogeometeorological disasters in the metropolitan area of São Paulo: a review. Ann NY Acad Sci 1472:5–20. https://doi.org/10.1111/nyas.14075

McGregor GR, Ferro CAT, Stephenson DB (2005) Projected changes in extreme weather and climate events in Europe. In: Kirch W, Bertollini R, Menne B (eds) Extreme weather events and public health responses. Springer, Berlin, Heidelberg. https://doi.org/10.1007/3-540-28862-7_2

Meehl GA, Stocker TF, Collins WD, et al (2007) Global climate projections. In: Solomon S, Qin D, Manning M, Chen Z, Marquis M, Averyt KB, Tignor M, Miller HL (eds) Climate Change 2007: the physical science basis. Contribution of Working Group I to the Fourth Assessment Report of the Intergovernmental Panel on climate change. Cambridge University Press, Cambridge, UK, and New York, NY, pp 747–845

Morris L, Hassan J, Rauhala E (2021) Death toll from European floods climbs to more than 150. Accessed 5 Aug 2021. https://www.washingtonpost.com/world/2021/07/16/europe-flooding-deaths-germany-belgium/

Mueller B, Seneviratne S (2012) Hot days induced by precipitation deficits at the global scale. PNAS 109(31):12398–12403. https://doi.org/10.1073/pnas.1204330109

Narsey SY, Brown JR, Colman RA (2020) Climate change projections for the Australian monsoon from CMIP6 models. Geophys Res Lett. https://doi.org/10.1029/2019GL086816

NOAA (2021) NOAA National Centers for Environmental Information, State of the Climate: Global Climate Report for Annual 2019. Published online January 2020. Retrieved 5 Aug 2021. https://www.ncdc.noaa.gov/sotc/global/201913

Nõges T, Nõges P, Cardoso AC (2010) Review of published climate change adaptation and mitigation measures related with water. JRC 62545 EUR 24682 EN. Accessed 01 Aug 2021. doi: https://doi.org/10.2788/18203

Pascale S, Kapnick SB, Delworth TL, Cooke WF (2020) Increasing risk of another Cape Town "Day Zero" drought in the 21st century. PNAS 117(47):29495–29503. https://doi.org/10.1073/pnas.2009144117

Philip N (2020) Climate change made Australia's devastating fire season 30% more likely. Nature. https://doi.org/10.1038/d41586-020-00627-y

Rastogi D, Lehner F, Ashfaq M (2020) Revisiting recent US heat waves in a warmer and more humid climate. Geophys Res Lett. https://doi.org/10.1029/2019GL086736

Saeed F, Schleussner CF, Ashfaq M (2021a) Deadly heat stress to become commonplace across South Asia already at 15°C of global warming. Geophys Res Lett. https://doi.org/10.1029/2020GL091191

Saeed F, Schleussner CF, Almazroui M (2021b) From Paris to Makkah: heat stress risks for Muslim pilgrims at 1.5°C and 2°C. Environ Res Lett 16:024037

Samenow J (2021) How weather patterns conspired for a flooding disaster in Germany. Accessed 5 Aug 2021. https://www.washingtonpost.com/weather/2021/07/16/weather-pattern-climate-germany-flooding/

Schiermeier (2021) Climate change made North America's deadly heatwave 150 times more likely. Accessed 5 Aug 2021. https://www.nature.com/articles/d41586-021-01869-0

Scoccimarro E, Gualdi S (2020) Heavy daily precipitation events in the CMIP6 worst-case scenario: projected twenty-first-century changes. J Clim 33:7631–7742

Seneviratne SI, Hauser M (2020) Regional climate sensitivity of climate extremes in CMIP6 versus CMIP5 multimodel ensembles. Earth Futur. https://doi.org/10.1029/2019EF001474

Seneviratne S, Nicholls N, Easterling D, et al (2012) Changes in climate extremes and their impacts on the natural physical environment. In: Field CB, Barros V, Stocker TF, Qin D, Dokken DJ, Ebi KL, Mastrandrea MD, Mach KJ, Plattner G-K, Allen SK, Tignor M, Midgley PM (eds) Managing the risks of extreme events and disasters to advance climate change adaptation, a special report of Working Groups I and II of the Intergovernmental Panel on Climate Change (IPCC). Cambridge University Press, Cambridge, UK, and New York, NY, USA, pp 109–230

Sillmann J, Kharin VV, Zhang X, Zwiers FW, Bronaugh D (2013) Climate extremes indices in the CMIP5 multimodel ensemble: part 1. Model evaluation in the present climate. J Geophys Res 118(4):1716–1733. https://doi.org/10.1002/jgrd.50203

Singh J, Ashfaq M, Skinner CB et al (2021) Amplified risk of spatially compounding droughts during co-occurrences of modes of natural ocean variability. Clim Atmos Sci 4:7. https://doi.org/10.1038/s41612-021-00161-2

Smith AB, Matthews JL (2015) Quantifying uncertainty and variable sensitivity within the US billion-dollar weather and climate disaster cost estimates. Nat Hazard 77:1829–1851. https://doi.org/10.1007/s11069-015-1678-x

Sousa PM, Blamey RC, Reason CJC, Ramos AM, Trigo RM (2018) The 'Day Zero' Cape Town drought and the poleward migration of moisture corridors. Environ Res Lett 13:124025. https://doi.org/10.1088/1748-9326/aaebc7

Srivastava A, Grotjahn R, Paul AU (2020) Evaluation of historical CMIP6 model simulations of extreme precipitation over contiguous US regions. Weather Clim Extrem 29:100268. https://doi.org/10.1016/j.wace.2020.100268

Travis WR (2014) Weather and climate extremes: pacemakers of adaptation? Weather Clim Extrem 5–6:29–39. https://doi.org/10.1016/j.wace.2014.08.001

Trenberth KE (2011) Changes in precipitation with climate change. Clim Res 47:123–138. https://doi.org/10.3354/cr00953

Trenberth KE, Jones PD, Ambenje P et al (2007) Observations: surface and atmospheric climate change. In: Solomon S, Qin D, Manning M, Chen Z, Marquis M, Averyt KB, Tignor M, Miller HL (eds) Climate change 2007: the physical science basis. Contribution of Working Group I to the Fourth Assessment Report of the Intergovernmental Panel on climate change. Cambridge University Press, Cambridge, UK, and New York, NY, pp 235–336

Turkey (2021) Turkey: Foreign tourists evacuated as wildfires threaten resorts. Accessed 5 Aug 2021. https://www.bbc.com/news/world-europe-58043912

US and Canada heatwave (2021) US and Canada heatwave: Pacific Northwest sees record temperatures. Accessed 5 Aug 2021. https://www.bbc.com/news/world-us-canada-57626173

Vogel MM, Hauser M, Seneviratne S (2020) Projected changes in hot, dry and wet extreme. Environ Res Lett 15:094021. https://doi.org/10.1088/1748-9326/ab90a7/pdf

Wehner M, Gleckler P, Lee J (2020) Characterization of long period return values of extreme daily temperature and precipitation in the CMIP6 models: part 1, model evaluation. Weather Clim Extrem 30:100283. https://doi.org/10.1016/j.wace.2020.100283

WMO (2021) Water-related hazards dominate disasters in the past 50 years. Published 23 July 2021. Accessed 5 Aug 2021. https://public.wmo.int/en/media/press-release/water-related-hazards-dominate-disasters-past-50-years

Fan X, Miao C, Duan Q, Shen C, Wu Y (2020) The performance of CMIP6 versus CMIP5 in simulating temperature extremes over the global land surface. J Geophys Res Atmos. https://doi.org/10.1029/2020JD033031

Zhang R, Sun C, Zhu J et al (2020) Increased European heat waves in recent decades in response to shrinking Arctic sea ice and Eurasian snow cover. npj Clim Atmos Sci 3:7. https://doi.org/10.1038/s41612-020-0110-8

Zhou BT, Wen QH, Xu Y, Song L, Zhang X (2014) Projected changes in temperature and precipitation extremes in China by the CMIP5 multimodel ensembles. J Clim 27:6591–6611. https://doi.org/10.1175/JCLI-D-13-00761.1